Neuron 50, 697–709, June 1, 2006 ©2006 Elsevier Inc. DOI 10.1016/j.neuron.2006.04.033

A Multireceptor Genetic Approach Uncovers an Ordered Integration of VNO Sensory Inputs in the Accessory Olfactory Bulb

Shlomo Wagner,[1,*] Amy L. Gresser,[2] A. Thomas Torello,[2] and Catherine Dulac[2,*]
[1] Department of Neurobiology
Hebrew University
Jerusalem 91904
Israel
[2] Howard Hughes Medical Institute
Department of Molecular and Cellular Biology
Harvard University
Cambridge, Massachusetts 02138

Summary

Pheromone detection by the vomeronasal organ (VNO) is thought to rely on activation of specific receptors from the *V1R* and *V2R* gene families, but the central representation of pheromone receptor activation remains poorly understood. We generated transgenic mouse lines in which projections from multiple populations of VNO neurons, each expressing a distinct *V1R*, are differentially labeled with fluorescent proteins. This approach revealed that inputs from neurons expressing closely related *V1R*s intermingle within shared, spatially conserved domains of the accessory olfactory bulb (AOB). Mitral cell-glomerular connectivity was examined by injecting intracellular dyes into AOB mitral cells and monitoring dendritic contacts with genetically labeled glomeruli. We show that individual mitral cells extend dendrites to glomeruli associated with different, but likely closely related, *V1R*s. This organization differs from the labeled line of OR signaling in the main olfactory system and suggests that integration of information may already occur at the level of the AOB.

Introduction

In many species, pheromones play an essential role in promoting and regulating sexual and social interactions. Recent evidence has shown that, in rodents, the detection of pheromones leading to behavioral and endocrine changes relies on the activity of both the main olfactory system and the vomeronasal system (Boehm et al., 2005; Dulac, 2005; Leypold et al., 2002; Lin da et al., 2005; Mandiyan et al., 2005; Stowers et al., 2002; Yoon et al., 2005).

How is the activation of defined sets of pheromone receptors encoded in the brain and translated into specific behavioral and physiological responses? While fundamental principles of information coding have been uncovered in the main olfactory system, the basic rules governing vomeronasal sensory processing have not yet been clearly established. In the main olfactory system, axons originating in the main olfactory epithelium (MOE) project to glomeruli in the main olfactory bulb (MOB) where they synapse with mitral and tufted cells, the bulb output neurons. Molecular and genetic studies have demonstrated that olfactory sensory neurons expressing the same olfactory receptor (OR) innervate one or a few pairs of glomeruli at fixed locations in the MOB (Mombaerts et al., 1996; Ressler et al., 1994; Vassar et al., 1994) while mitral and tufted cells project one apical dendrite into a single glomerulus in the MOB glomerular layer. This organization generates a "labeled line" of information processing (Luo and Katz, 2004) in which each mitral cell processes and transfers to higher brain centers excitatory inputs generated by the activation of a given OR and modulated by cross-talk between mitral cells and local interneurons.

VNO neurons send axonal projections to the accessory olfactory bulb (AOB). Sensory neurons located in the apical layer of the VNO neuroepithelium each express a single member of the *V1R* family of VNO receptors (VRs) and project to the anterior AOB, while neurons in the basal layer express receptors of the *V2R* family and project to the posterior AOB (Dulac and Torello, 2003). Members of the *V1R* and *V2R* gene families exhibit a high degree of sequence diversity and are grouped into distinct subfamilies or clades which are extremely divergent from each other phylogenetically (Rodriguez et al., 2002; Yang et al., 2005). While members of a given clade are highly similar, the high degree of divergence between *VR* genes belonging to different clades contrasts sharply with the smooth continuum in *OR* sequence variability, in which the whole space of sequence diversity is spanned.

The organizational principles of the vomeronasal sensory representation in the AOB remain unclear. VNO neurons expressing the same VR innervate 6 to 30 glomeruli, forming a complex pattern of innervation that seems roughly preserved between individual animals (Belluscio et al., 1999; Del Punta et al., 2002; Rodriguez et al., 1999) and that differs for neurons expressing distinct receptors. Compared to the simple representation of glomeruli with stereotyped positions in the MOB, the AOB representation, presumably aimed at translating stimulation of discrete sets of VNO receptors into fixed patterns of behavior, appears surprisingly complex and prone to individual variations. This suggests that the representation of VNO inputs in the AOB may obey a higher-order organization yet to be identified. In an additional contrast with the organization of the main olfactory system, individual AOB mitral cells have been shown to send multiple apical dendrites to a collection of three to nine AOB glomeruli (Takami and Graziadei, 1990) raising the possibility that excitatory inputs originating from populations of VNO neurons expressing different *VR*s may converge onto individual AOB mitral cells. This sensory representation would differ strikingly from that of the main olfactory system and instead would resemble that of the moth antennal lobe, in which output neurons have been shown to integrate multiple pheromone signals collected in distinct glomeruli (Kanzaki et al., 1989; Sadek et al., 2002; Vickers and Christensen, 2003). An initial report, however, showed some AOB mitral cells projecting dendrites to glomeruli receiving identical

*Correspondence: shlomo@lobster.ls.huji.ac.il (S.W.); dulac@fas.harvard.edu (C.D.)

receptor inputs (Del Punta et al., 2002), raising the broad issue of the logic of VNO connectivity in the AOB.

We have aimed here at deciphering the general principles of information processing in the AOB: what rules, if any, govern the pattern of VNO projections to the AOB and of dendritic connectivity with AOB mitral cells? What are the functional implications for the coding of pheromone signals leading to behavioral changes?

We developed a genetic and imaging paradigm to visualize, at a large scale, the relative positions of AOB glomeruli innervated by distinct populations of VNO neurons and the patterns of mitral cell-glomerular connectivity. Our results suggest that, in contrast to the labeled lines of information flow demonstrated in the MOB and based on individual OR signaling, the AOB is organized as an integration center for inputs originating from subsets of closely related *VR* receptors. We show here that the AOB glomerular layer forms a receptor subfamily-based glomerular map according to which glomeruli originating from neurons expressing receptors of a given subfamily are intermingled within shared domains with specific spatial coordinates. Moreover, we demonstrate that AOB mitral cells can collect information from multiple *V1R*s, presumably members of the same subfamily. From these distinctive features, the vomeronasal sensory representation is strikingly different from that of the main olfactory system. We propose here that the AOB organization provides an identity rather than a simple spatial code, which may offer a suitable organization for the coding of pheromonal blends.

Results

Construction of a Multireporter Transgenic Mouse Line

In order to investigate the broad organization principles of VNO projection to the AOB, we generated a transgenic mouse line in which multiple populations of VNO neurons, each expressing a different *V1R*, are differentially labeled with fluorescent proteins. This approach offered the opportunity to directly visualize, on a large scale, the relative positions of AOB glomeruli innervated by distinct populations of VNO neurons.

BAC 398H20, containing an array of six functional *V1R* genes, was identified from screening a BAC library with a mix of receptor probes. In an initial experiment, the BAC 398H20 was modified by insertion of the reporter cassette *IRES-tau-YFP* downstream of the *V1Ra1* coding sequence. The SW1M transgenic mouse line generated with this construct was analyzed for YFP expression in the VNO. *YFP*-expressing cells were found in the VNO neuroepithelium dissected from the SW1M line, indicating expression of the transgene in a subpopulation of VNO neurons. The loci of two receptor genes, *V1Ra1* and *V1Rb1*, was previously modified by gene targeting (Belluscio et al., 1999) that introduced an *IRES-tau-lacZ* cassette downstream of the receptor coding sequence, generating the mouse lines VN12/T40 and VN2/66, respectively. To validate the accuracy of BAC transgenic modification compared to gene targeting by homologous recombination, we generated compound heterozygotes from a cross of the SW1M and VN12/T40 lines. In these mice, the *V1Ra1* gene is located in three different loci: the wild-type allele, the targeted *V1Ra1-tau-lacZ* allele, and the transgenic *V1Ra1-tau-YFP* allele (Figure 1A). Genomic Southern analysis led us to estimate the presence of two to three copies of the BAC transgene in the genome of the SW1M line. From known mechanisms of *OR* and *VR* gene regulation (Chess et al., 1994; Serizawa et al., 2000), a single receptor-expressing cell is expected to actively transcribe only one of its maternal, paternal, or transgenic alleles. Accordingly, two populations of labeled neurons could be detected in VNO slices from the compound heterozygotes (Figure 1B). In a 0.0550 mm^2 area of VNO neuroepithelium, we detected an average of 18 YFP-labeled neurons and ten *tau-lacZ*-expressing cells (three VNO slices from three animals). Thus, distinct populations of *V1Ra1*-expressing neurons, each recognized by the presence of a different reporter gene, can be distinguished as expected from an allelic choice of receptor transcription, and their relative ratios are consistent with the copy number of each allele in the genome of the compound heterozygotes. *OR*s and *VR*s are thought to play an instructive role in axonal projection to glomerular targets in the olfactory bulb (Belluscio et al., 1999; Conzelmann et al., 2001; Mombaerts et al., 1996; Rodriguez et al., 1999; Tsuboi et al., 1999). One would therefore expect that populations of VNO neurons expressing the same *V1R* from different alleles, each identified by a different reporter, would innervate common glomeruli in the AOB. Accordingly, analysis of 40 glomeruli in three different AOB preparations from compound heterozygote mice showed that both *V1Ra1*-expressing neuronal populations, visualized by either anti-β-galactosidase immunofluorescence (Figure 1C) or *tau-YFP* expression (Figure 1D), innervate shared glomeruli in the anterior AOB (Figure 1E). In contrast, SW1MxVN2/66 compound heterozygote mice contain YFP-positive *V1Ra1*-expressing cells and β-galactosidase-positive *V1Rb1*-expressing neurons that send axons to different targets in the AOB (Figures 1F–1H). Thus, receptor locus modification by BAC transgenesis or gene targeting leads to similar receptor expression patterns and unaltered glomerular innervation.

To determine the relative spatial positions of glomeruli innervated by members of different *V1R* gene subfamilies, we further modified the SW1M BAC by inserting two additional reporter cassettes: *IRES-tau-CFP* downstream of the *V1Rb1* coding sequence and *IRES-vamp-DsRed1* downstream of *V1Ra3*. Note that both the *V1Ra1* and *V1Ra3* genes belong to the *V1Ra* subfamily while the *V1Rb1* gene belongs to the *V1Rb* subfamily. This construct (Figure 2A) was used to generate the SW3M transgenic line. When crossed with the VN12/T40 line, four different populations of VNO neurons, each expressing a different marker, could be detected (Figures 2B–2G). In a 0.0550 mm^2 area of VNO neuroepithelium, we identified an average of 23 CFP-labeled *V1Rb1*-expressing cells, 35 DsRed1-labeled *V1Ra3*-expressing cells, and 43 YFP-labeled *V1Ra1*-expressing cells resulting from transgene expression, as well as 12 *tau-lacZ*-positive *V1Ra1*-expressing cells from gene targeting (three VNO slices from three animals). We interpreted the high number of YFP-labeled cells compared to that of *tau-lacZ*-expressing cells as resulting from the higher copy number of the transgene locus in

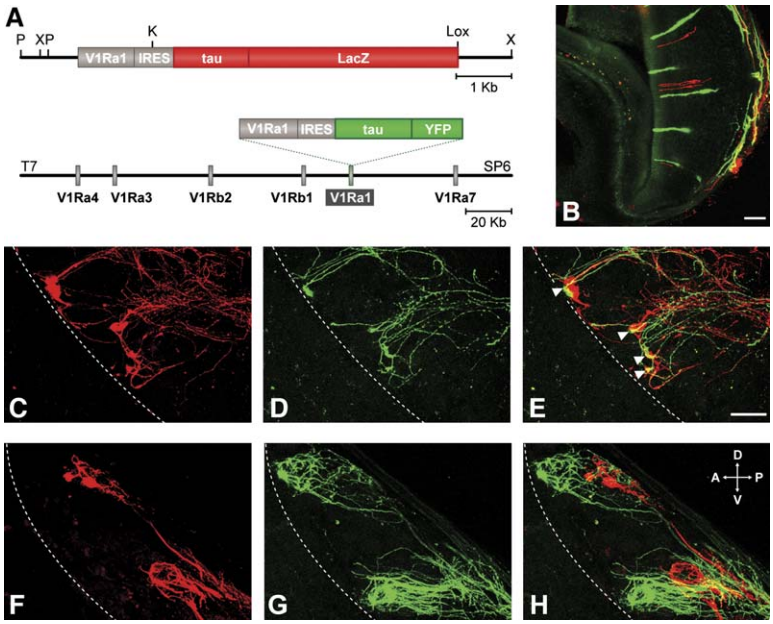

Figure 1. V1Ra1 Genetic Labeling Is Comparable in Mice Generated by Gene Targeting and BAC Transgenics

(A) Constructs used for generation of VN12-IRES-tau-lacZ (VN12-ITL) gene targeted mice (top, Belluscio et al., 1999) and SW1M BAC transgenic mice (bottom). In each of the mouse lines, the *V1Ra1* gene was coupled to a different reporter gene by an internal ribosomal entry site (IRES) sequence.

(B) Coronal VNO slice from a SW1MxVN12-ITL compound heterozygote mouse showing two nonoverlapping populations of *YFP*-expressing cells (green) and immunohistochemically stained *lacZ*-expressing cells (red).

(C–E) Parasagittal AOB slice from a similar mouse. Stained *lacZ*-expressing (C) and *YFP*-expressing (D) VNO fibers converge on the same glomerular targets (arrowheads, [E]). Dashed lines mark the ventral border of the glomerular layer.

(F–H) Parasagittal AOB slice from an SW1xVN2-ITL compound heterozygote mouse where different receptor genes (*V1Ra1* and *V1Rb1*) are coupled to different reporter genes. *lacZ*-expressing fibers innervate different glomerular targets than *YFP*-expressing fibers. Note the consistent spatial relationship between the two types of targets in both the anterior (left) and posterior (right) genetically labeled domains.

Directions: A, anterior; P, posterior; D, dorsal; V, ventral. Scale bars, 50 μm.

the SW3M line compared to that of the targeted allele (data not shown). The 2:3:4 ratio of CFP-, DsRed1-, and YFP-expressing cells reflects the fact that different *V1R* receptors are naturally expressed in varying numbers of VNO neurons (Belluscio et al., 1999).

Analysis of olfactory bulbs taken from compound heterozygote mice showed that all glomeruli innervated by *tau-lacZ*-positive *V1Ra1*-expressing cells are also innervated by YFP-labeled *V1Ra1*-expressing neurons (22 glomeruli from three animals, Figures 2H–2J).

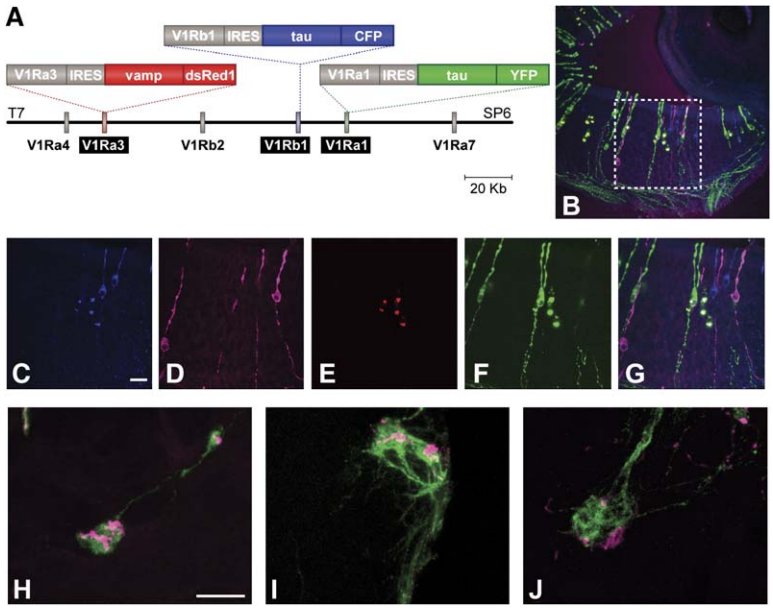

Figure 2. VNO Receptor Gene Expression and Wiring Logic Is Preserved in the Multireporter BAC-Transgenic Mouse Line

(A) BAC construct used in generation of SW3M transgenic mice.

(B) Coronal VNO slice from a SW3MxVN12-ITL compound heterozygote mouse showing four nonoverlapping, genetically labeled neuronal populations. Immunohistochemically-stained (Cy5) *lacZ*-expressing cells are shown in pink, *YFP*-expressing cells in green, and *CFP*-expressing cells in blue. *DsRed1*-expressing *V1Ra3*-positive fibers are seen as white dots. Note that the *lacZ*- and *YFP*-expressing cells express the same receptor gene (*V1Ra1*).

(C–F) Enlargement of area defined by dashed rectangle in (B) shown for single confocal tracks: (C) CFP, (D) Cy5, (E) DsRed1 and (F) YFP. Note that aggregated DsRed1 is seen in the CFP and YFP tracks as well as in its own.

(G) Merged view of panels (C–F).

(H–J) *V1Ra1*-innervated glomeruli in parasagittal anterior AOB slices from three compound heterozygote mice. Both neuronal populations, each expressing the *V1Ra1* receptor gene from a different modified locus, innervate the same glomeruli. Note that the *lacZ*- and *YFP*-expressing fibers are compartmentalized within each glomerulus.

Scale bars, 25 um.

The Multireceptor Organization of the AOB Glomerular Layer

Because it contains three labeled neuronal populations, each expressing a distinct receptor from one of two *V1R* subfamilies, the SW3M line provides a valuable tool to examine the internal organizational principles of the AOB glomerular map. To monitor the relative locations of the differentially labeled glomeruli, we used confocal microscopy to examine 100 μm parasagittal vibratome slices of fixed olfactory bulbs. This design permits nearly all labeled glomeruli to be confined to a series of four slices and allowed us to systematically assess and compare the location of labeled glomeruli within a given bulb and across individuals. As noted previously (Belluscio et al., 1999), definition of individual AOB glomeruli is less straightforward than that of MOB glomeruli, which are surrounded by periglomerular neurons and glia. Nonetheless, examination of sequential optical slices through the AOB allowed us to follow labeled axons from the point of AOB entry to their eventual termini at the basket-like fiber clumps characteristic of glomeruli. Figures 3A–3D show a series of parasagittal slices from the same bulb. *Tau-YFP*- expressing and *tau-CFP*-expressing fibers emerge from the medial aspect of the bulb and spread to glomerular targets in the AOB. Since vamp is a synaptic protein, no red fibers are observed, but the glomeruli occupied by red *vamp-DsRed1*-expressing terminals are clearly seen.

Examination of equivalent AOB slices across different preparations enabled us to compare the locations of genetically labeled glomeruli and highlighted a clear pattern of labeled glomeruli that persists across individuals, suggesting a nonrandom distribution of glomeruli of a given type both within the AOB glomerular layer and relative to the positions of other identified glomeruli (Figures 3E–3H).

To further investigate the broad features of this multireceptor glomerular map, we quantified the relative positions of *V1Ra1*-, *V1Ra3*-, and *V1Rb1*-associated glomeruli. We systematically measured the x and y coordinates of each glomerulus on a Cartesian plane in which the anterior-posterior axis is parallel to the x axis, the dorsal-ventral axis is parallel to the y axis and the anterior-dorsal tip of the anterior AOB occupies the origin. Twelve preparations were analyzed (six male, six female) with each preparation containing an average of (mean ± SD) 11.1 ± 3.0 *V1Ra1*, 12.0 ± 4.2 *V1Ra3*, and 4.2 ± 1.6 *V1Rb1* glomeruli.

Each of the four 100 μm parasagittal slices was analyzed separately across the 12 preparations. To reduce the variability in the size and orientation of sections between preparations, we calculated the normalized positions of glomeruli by dividing the x and y coordinate values of each glomerulus by the total length and local thickness of the AOB glomerular layer, respectively.

In agreement with previous observations (Belluscio et al., 1999), each set of labeled glomeruli appears to be clustered in discrete areas, or domains, with conserved positions along the x and y axes of the glomerular layer (Figures 3E–3H; Figure 4). Moreover, new features of the glomerular map emerged from the analysis of the relative positions of labeled glomeruli. Along the y axis, *V1Rb1* glomeruli appear distinctively separated from *V1Ra1* and *V1Ra3* glomeruli, occupying a more

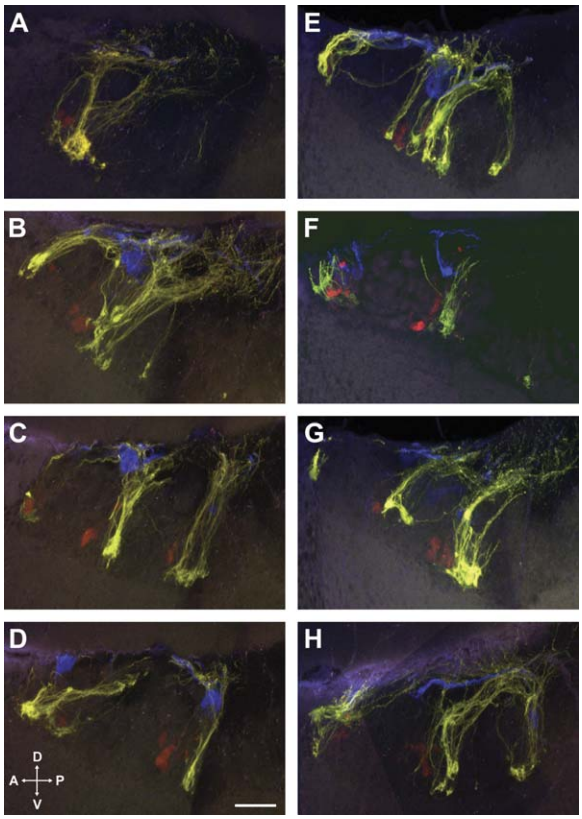

Figure 3. Multireporter Labeling of V1R-Expressing Neuron Terminals in the AOB of SW3M Mice Reveals a Fixed Innervation Pattern that Persists across Individuals

(A–D) Sequential 100 μm parasagittal anterior AOB slices from a SW3M mouse arranged from medial (A) to lateral (D). Note the columnar organization in which *CFP*-expressing fibers (blue) form glomeruli in the dorsal area while *YFP*-expressing fibers (yellow) and *DsRed1*-expressing terminals (red) form glomeruli in the ventral area.

(E–H) The third slice from four equivalent series taken from different SW3M mice (two males and two females) showing consistent arrangement of labeled glomeruli across individuals.

Scale bar, 80 μm.

dorsal position within the glomerular layer. If 0 represents the dorsal edge of the AOB glomerular layer and 1 represents the ventral edge, *V1Rb1* glomeruli lie on average at coordinates between 0.2 and 0.4, while both *V1Ra1* and *V1Ra3* glomeruli lie between 0.5 and 0.8. More precise measurements were obtained by examination of each of the four AOB slices individually across all preparations. Figure 4A (left) shows the distribution along the normalized y axis of all labeled glomeruli in the third slice of all 12 preparations. The mean positions of the various glomerular clusters are as follows: *V1Ra1* = 0.77 ± 0.18 (n = 33), *V1Ra3* = 0.67 ± 0.14 (n = 40), and *V1Rb1* = 0.33 ± 0.16 (n = 16). Approximately two-thirds of glomeruli lie within one standard deviation of the mean position (*V1Ra1*, 76%; *V1Ra3*, 70%; *V1Rb1*, 63%). The dorso-ventral segregation of the *V1Rb1* glomeruli from the *V1Ra1* and *V1Ra3* glomerular clusters is highly significant ($p < 0.00001$, one-tailed unpaired t test) while the difference between the *V1Ra1* and *V1Ra3* clusters is not significant ($p > 0.1$, one-tailed unpaired t test).

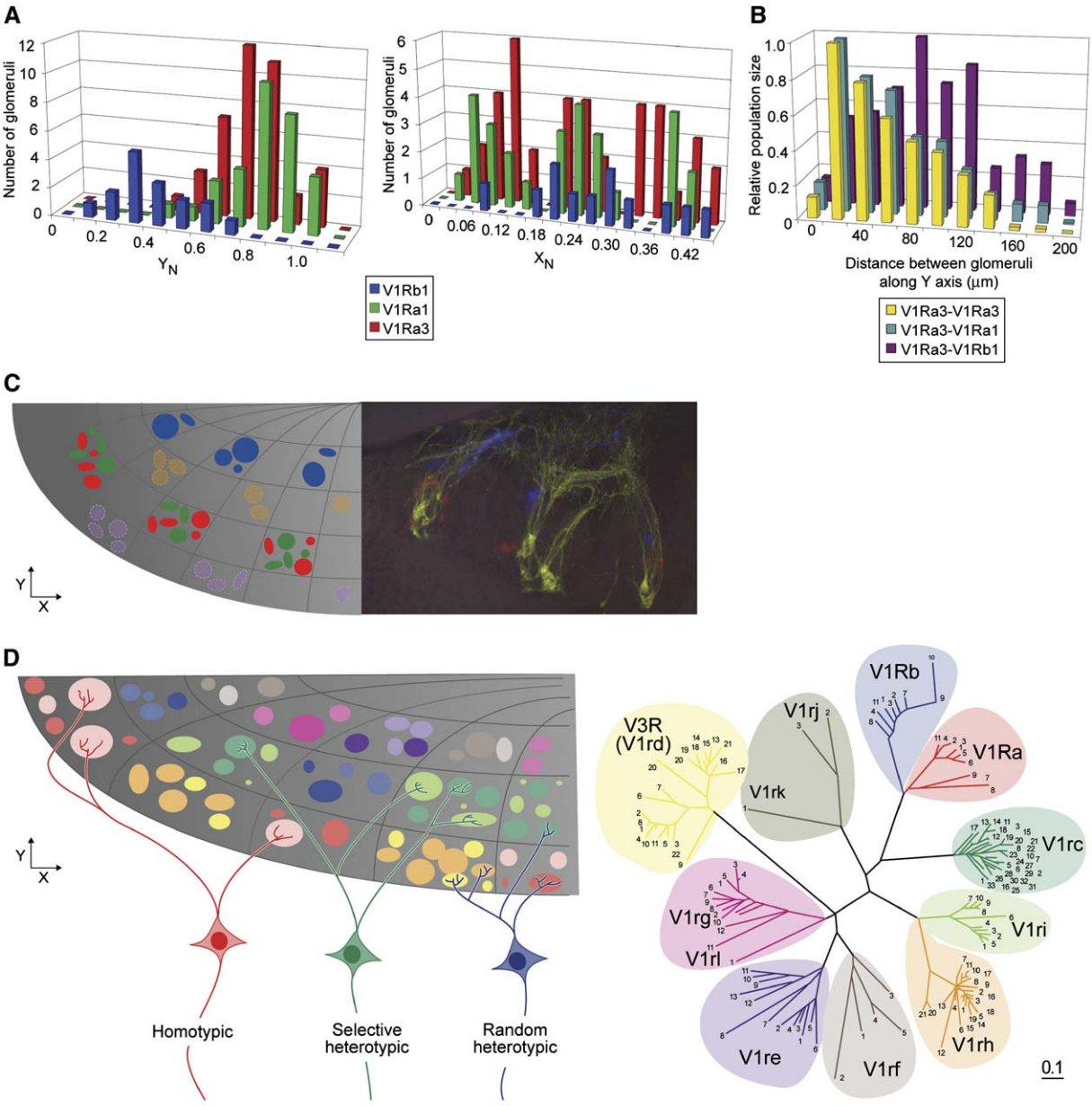

Figure 4. Quantification of Positions for Labeled Glomeruli Suggests a Grid-Like Organization of the AOB Glomerular Layer According to Receptor Gene Subfamily

(A) Positions of labeled glomeruli along the dorsal-ventral (left) and anterior-posterior (right) axes in AOB parasagittal slice #3. Values are normalized such that 0 corresponds to the dorsal or anterior boundary of the AOB glomerular layer and 1 corresponds to the ventral or posterior boundary. While along the anterior-posterior axis all labeled glomeruli are located in the same three domains, along the dorsal-ventral axis *V1Rb1* glomeruli are located more dorsally relative to the common location of *V1Ra1* and *V1Ra3* glomeruli.

(B) Distribution of distances along the dorsal-ventral AOB axis between pairs of labeled glomeruli.

(C) Model for *V1R* subfamily-based organization of glomeruli in the anterior AOB. Glomeruli innervated by neurons expressing *V1Ra1* (green) and *V1Ra3* (red) are grouped together in three ventral domains while those formed by *V1Rb1*-expressing neurons (blue) are located in separate, more dorsal domains. Circles indicate the nonoverlapping domains occupied by *V1Re4* (purple) and *V1Rh7* or *V1Rh15* (orange) glomeruli (see Figure S1).

(D) Extrapolation of the model shown in (C) to include glomeruli formed by neurons expressing *V1R*s from all subfamilies (left) as classified in the phylogenetic tree (right). Three possible schemes for connectivity of mitral cells to these glomeruli are shown: homotypic, selective heterotypic, and random heterotypic.

In an independent set of measurements, we monitored the distances along the y axis between all pairs of labeled glomeruli located in each slice (Figure 4B). Similar results were obtained for all three sets of labeled glomeruli when distances were calculated between glomeruli of the same type. The average distance between *V1Ra1*-positive glomeruli is 62.6 ± 3.4 μm (n = 185); between *V1Ra3*-positive glomeruli, it is 53.0 ± 2.7 μm (n = 225); and between *V1Rb1*-positive glomeruli, it is 51.8 ± 9.2 μm (n = 22). There is no significant difference between distances for the *V1Rb1* population and either of the other populations ($p > 0.1$, one-tailed unpaired

t test) while the difference between the *V1Ra1* and *V1Ra3* populations is barely significant ($p < 0.05$, one-tailed unpaired t test). These results suggest a similar distribution along the y axis for all three glomerular populations. In contrast, analysis of distances between glomeruli associated with different receptors revealed a preferential distribution of specific types of glomeruli relative to others. Distances separating *V1Ra3*- and *V1Ra1*-positive glomeruli (Figure 4B teal; 53.0 ± 2.7 μm, n = 225) appear identical to distances between *V1Ra3*-positive glomeruli (Figure 4B yellow; 56.4 ± 2.2 μm, n = 413), but distances between *V1Ra3* and *V1Rb1* glomeruli are very different (Figure 4B purple; 82.8 ± 4.0 μm, n = 150; $p < 0.0001$, one-tailed unpaired t test) and peak around 100 μm instead of 40 μm, as for the other distributions. Thus, *V1Ra1* and *V1Ra3* glomeruli are clustered together along the y axis such that there is an equal chance of a *V1Ra3* or *V1Ra1* glomerulus lying close to one glomerulus of its own type or one of the other type while *V1Rb1* glomeruli are located in a different zone of the glomerular layer.

Along the anterior-posterior or x axis, all labeled glomeruli are located within three domains, or columns where *V1Ra1*- and *V1Ra3*-expressing terminals innervate ventral glomeruli and *V1Rb1*-expressing terminals innervate more dorsal targets. Interestingly, *V1Ra1*-expressing fibers seem to reach their glomerular targets through *V1Rb1* domains, creating the impression of radial columns containing all three types of labeled glomeruli (Figure 3). Figure 4A (right) shows the distributions of normalized x values for all labeled glomeruli in slice #3 of all preparations. Despite slight orientation differences between the different preparations, all three glomerular populations occupy similar domains along the anterior-posterior axis (mean ± SEM): domain 1: *V1Ra1* 0.07 ± 0.04 (n = 11), *V1Ra3* 0.09 ± 0.04 (n = 15), *V1Rb1* 0.09 ± 0 (n = 1); domain 2: *V1Ra1* 0.22 ± 0.03 (n = 11), *V1Ra3* 0.22 ± 0.03 (n = 10), *V1Rb1* 0.24 ± 0.05 (n = 8); domain 3: *V1Ra1* 0.43 ± 0.06 (n = 11), *V1Ra3* 0.37 ± 0.05 (n = 15), *V1Rb1* 0.45 ± 0.04 (n = 3), where 0 represents the anterior AOB edge and 1 the posterior edge of the AOB. Considering the glomeruli included in each domain separately, approximately two-thirds of glomeruli lie within one standard deviation of the mean position for that domain (*V1Ra1*, 61%; *V1Ra3*, 63%; *V1Rb1*, 69%).

In summary, all labeled glomeruli are located within the same three columns along the anterior-posterior axis, but *V1Ra1* and *V1Ra3* glomeruli are intermingled in a ventral domain while *V1Rb1* glomeruli are located in a separate dorsal strip (Figure 4C). Thus, our results appear consistent with a broad organizational scheme in which the AOB glomerular layer is subdivided into a clade-based grid such that axonal projections of neurons expressing receptors from the same subfamily are intermingled within shared glomerular domains while projections from neurons expressing receptors belonging to different subfamilies occupy distinct domains with specific spatial coordinates.

To further document these results, three independent transgenic mouse lines were generated in which BACs containing the loci of the *V1Re4*, *V1Rh7*, and *V1Rh15* receptor genes were individually modified by insertion of reporter cassettes. The relative position of each glomerulus type was assessed by crossing the corresponding transgenic line with the VN12/T40 line, in which the *V1Ra1* locus has been modified by gene targeting. This analysis shows clusters of *V1Re4*-positive glomeruli occupying a position adjacent to but not overlapping with *V1Ra*-related projections, while both *V1Rh7* and *V1Rh15* glomeruli occupy a similar dorso-lateral position distinct from that of *V1Ra*-, *V1Rb*-, and *V1Re*-related domains (see Figure 4C and Figures S1A–S1C in the Supplemental Data).

Quantification of glomerular positions along the x and y axes (Figure S1D) further documents the existence of multiple nonoverlapping projection domains in the anterior AOB, each associated with a different *V1R* subfamily. Comparing across glomeruli in all slices (*V1Re4*, n = 65; *V1Rh7*, n = 43; *V1Rh15*, n = 62), we detected no significant difference in the positions of *V1Rh7*- and *V1Rh15*-associated glomeruli ($p > 0.1$, two-tailed unpaired t test), but the locations of *V1Re4*-positive glomeruli are significantly different ($p < 0.0001$, two-tailed unpaired t test). In addition, domains occupied by *V1Ra* (n = 328) and *V1Rb1* (n = 57) glomeruli are significantly different from those of either *V1Re4* or *V1Rh* glomeruli ($p < 0.005$, two-tailed unpaired t test). Along the anterior-posterior axis, *V1Re4* and *V1Rh* glomeruli, like *V1Ra* and *V1Rb1* glomeruli, are divided into three domains. Considering the glomeruli in all slices (domain 1: *V1Re4*, n = 43; *V1Rh7*, n = 35; *V1Rh15*, n = 36; domain 2: *V1Re4*, n = 15; *V1Rh7*, n = 7; *V1Rh15*, n = 21; domain 3: *V1Re4*, n = 7; *V1Rh7*, n = 1; *V1Rh15*, n = 5), we saw no significant differences in the locations of the three domains between *V1Rh7* and *V1Rh15* glomeruli ($p > 0.1$, two-tailed unpaired t test). Between *V1Rh* and *V1Re4* glomeruli, there is no significant difference between the locations of second and third domains, but differences in the positions of the first domain are significant ($p < 0.001$, two-tailed unpaired t test). Domains occupied by *V1Ra* (domain 1, n = 88; domain 2, n = 156; and domain 3, n = 84) and *V1Rb1* (domain 1, n = 9; domain 2, n = 30; and domain 3, n = 18) glomeruli are all significantly different from those of *V1Rh* and *V1Re4* glomeruli ($p < 0.005$, two-tailed unpaired t test), with three exceptions: *V1Re4* domain 2 is not significantly different from domain 3 for *V1Ra* or *V1Rb1* ($p > 0.1$ and $p < 0.1$, respectively, two-tailed unpaired t tests). In addition, *V1Rh* domain 1 is not significantly different from *V1Rb1* domain 1 and *V1Rh* domain 2 is not significantly different from *V1Ra* domain 3 ($p > 0.1$, two-tailed unpaired t tests). These instances of insignificant differences between domains for different receptor types along the anterior-posterior axis do not correlate with a spatial overlap in the AOB, since the dorsal-ventral areas occupied by the receptors are significantly different. Thus, glomeruli formed by neurons expressing receptors from four different *V1R* subfamilies are clustered into multiple nonoverlapping AOB domains (Figure 4C). Figure 4D shows the hypothetical extrapolation of this model to all *V1R* subfamilies.

AOB Mitral Cell Connectivity with Distinct VNO Neuronal Populations

The specific arrangement of sensory projections to the AOB glomerular layer observed in our study is consistent with the existence of a receptor subfamily-based glomerular map. The functional significance of this map,

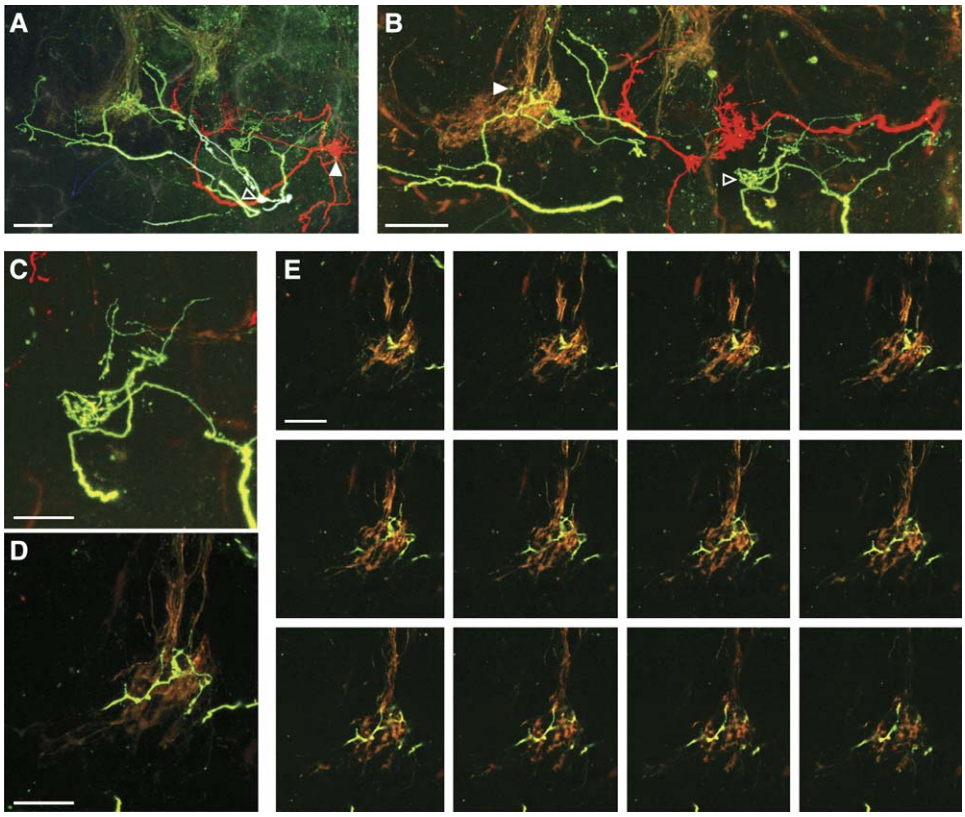

Figure 5. Dendritic Tufts from the Same Mitral Cell Innervate Both Labeled and Unlabeled Glomeruli

(A) Merged view of two sequential 100 μm semicoronal SW3M AOB slices containing mitral cells injected with LY (blue, cell body not seen), AF488 (green, cell body marked with hollow arrowhead) and AF568 (red, cell body marked with filled arrowhead).

(B) Second slice of the two shown merged in (A). Only green and red confocal channels are shown. One AF488-injected tuft within an unlabeled glomerulus is marked with a hollow arrowhead while another AF488-injected tuft within an YFP-labeled glomerulus is marked with a filled arrowhead.

(C and D) Higher magnification of the AF488-filled tufts from (B), labeled with hollow (C) and filled (D) arrowheads.

(E) Twelve 0.5 μm optical slices of the glomerulus shown in (D). Note the thin AF488-filled branches spreading into the YFP-labeled glomerulus. Scale bars for (A) and (B), 50 μm; scale bars for (C)–(E), 5 μm.

however, relies on the logic by which dendritic connections are established by mitral cells.

Differentially labeled glomeruli in the AOB of SW3M mice provide a useful tool for broad identification of mitral cell dendritic targets. We used various fluorescent dyes to fill multiple mitral cell bodies and processes in acute brain slices. In a first set of experiments, three random mitral cells identified by whole-cell patch-clamp in 400 μm semicoronal AOB slices were filled with one of the following dyes: lucifer yellow (LY), Alexa Fluor 488 (AF488) or Alexa Fluor 568 (AF568). After fixation, preparations were resliced into a series of four 100 μm slices that were examined separately. In most of these preparations, dye-filled mitral cells' processes are split across different slices.

To avoid the need to reconstitute dendritic arbors across slices, we performed a second set of experiments in which up to three mitral cells in 400 μm semicoronal or parasagittal slices were injected with different fluorescent dyes. After fixation, these slices were physically compressed to approximately 100 μm in thickness so that the dye-filled cell body and entire dendritic arbor could be observed in the same slice.

In both types of preparations, whole-cell patch-clamp recording prior to dye injection provided verification of the nature and singularity of the injected cells. Furthermore, we took great care to verify that a unique labeled cell body and connected dendrites could unambiguously be identified right after dye injection and throughout sample processing.

We examined approximately 150 dye-filled mitral cells: 40 cells were examined in the first set of experiments and 110 in the second. Among all injected cells, 11 filled cells showed dendritic tufts connected to a labeled glomerulus: seven to *V1Ra1*-positive glomeruli, three to *V1Ra3*-positive glomeruli, and one to both a *V1Ra1*-positive and a *V1Ra3*-positive glomerulus. In none of these cases did the cell send more than one tuft to the same type of glomerulus. Most neurons (seven cells) also sent at least one well-developed tuft to an unlabeled glomerulus, but in some cases (four cells) we did not observe any clear tufts in other glomeruli.

Figure 5 shows an example of the first type of preparation. One dendritic tuft from an AF488-filled mitral cell is seen branching within an unlabeled glomerulus, while a second tuft from the same cell is seen branching within

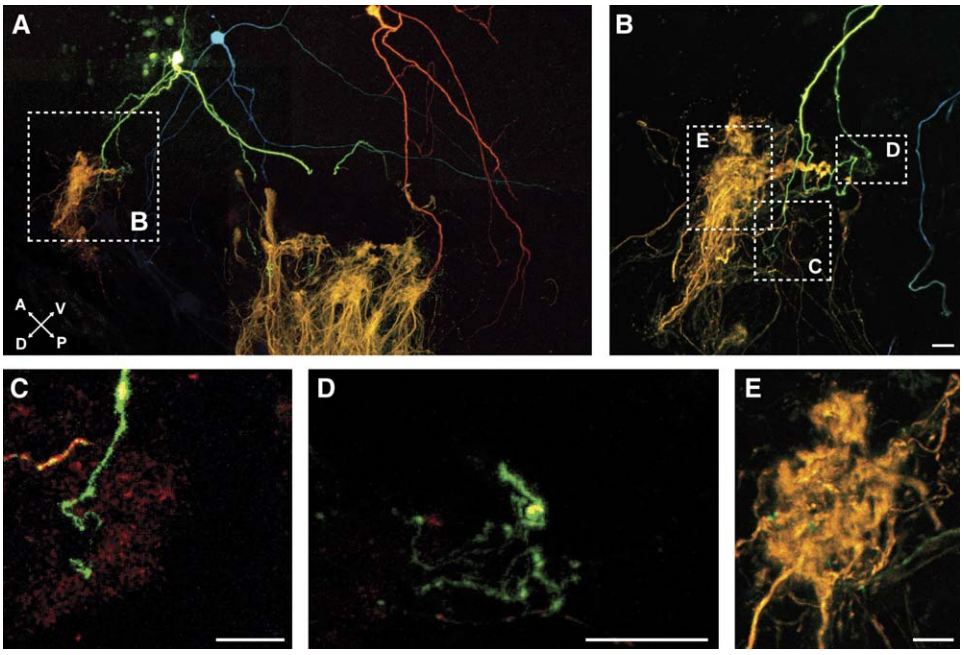

Figure 6. A Common Mitral Cell Innervates Glomeruli Formed by Neurons Expressing Different *V1R*s

(A) 400 μm parasagittal SW3M AOB slice containing mitral cells injected with LY (blue), AF488 (green) and AF568 (red) flattened to ~100 μm. The AF488-injected cell sends dendrites into both the anterior (left) and posterior (right) genetically labeled domains.
(B) Higher magnification of anterior domain shown in (A). Three AF488-labeled tufts are denoted by rectangles.
(C–E) Higher magnifications of the three tufts from (B). One tuft is seen entering a DsRed1-labeled glomerulus (C), another innervates an unlabeled glomerulus (D), and the third innervates an YFP-labeled glomerulus (E).
Scale bars, 2.5 um.

a *V1Ra1*-positive glomerulus. Thus, this mitral cell projects dendritic tufts to both YFP-labeled and unlabeled glomeruli.

Figure 6 shows an example from the second experimental strategy, in which three dye-filled mitral cells and their entire dendritic arbors reside in a single parasagittal slice. This AF488-filled cell projects tufts into three different glomeruli: a *V1Ra3*-positive glomerulus, a *V1Ra1*-positive glomerulus, and an unlabeled glomerulus. Thus, this mitral cell establishes connections with at least three types of glomeruli, two of which are related to the *V1Ra* family of receptors.

The Molecular Logic of Mitral Cell Connectivity

Our data clearly indicate that mitral cells receiving inputs from at least one glomerulus innervated by *V1Ra1*- or *V1Ra3*-expressing VNO neurons can also send dendritic tufts to glomeruli innervated by different receptors. In addition, Del Punta and colleagues (Del Punta et al., 2002) have shown that in some instances, none of which were encountered in our study, mitral cells may contact more than one glomerulus of the same type. Thus, it appears that the logic of mitral cell dendritic connectivity cannot be simply captured by either a homotypic or heterotypic model. Rather, we reasoned that, confronted with the organized grid of vomeronasal inputs described in the earlier part of this work, mitral cells may follow certain rules in establishing multidendritic connectivity with the aim of sampling specific classes of receptor activities. This wiring scheme, named here the selective heterotypic model, contrasts with a random heterotypic model according to which mitral cells would sample a random set of receptor inputs (Figure 4D).

Individual AOB mitral cells have been shown to extend dendrites that innervate glomeruli located at large distances from each other (Takami and Graziadei, 1990). We have shown that the organization of the AOB glomerular layer may follow a grid-like structure in which inputs originating from closely related receptors are clustered and spatially assigned to a few domains of the anterior AOB with specific radial and columnar coordinates. This spatial layout may provide a logical framework for mitral cell dendritic arborization. For example, mitral cell dendritic tufts may be restricted to the various domains across the anterior AOB that receive innervation from VNO neurons expressing *V1R* receptors of a given subfamily. To uncover such a high-order dendritic organization that would span the entire glomerular layer, we measured the distance from individual dye-filled dendritic tufts of labeled AOB mitral cells to the nearest *V1Ra1* or *V1Ra3* glomerulus (Figures 7A and 7B).

Distances between tufts and labeled glomeruli were measured for 21 labeled cells from the first set of dye-injection experiments that had at least two dendritic tufts in the AOB glomerular layer. For these cells, the number of tufts per cell ranged from between two to 11, with a median of three and a mean ± SD of 4.33 ± 0.59. Considering all of a given mitral cell's tufts as a group, we then calculated the average distance between those tufts and the nearest *V1Ra1/3*-positive glomerulus. Figure 7C (left) shows the distribution of these average distances. Remarkably, this distribution is bimodal, indicating the existence of two categories of mitral cells

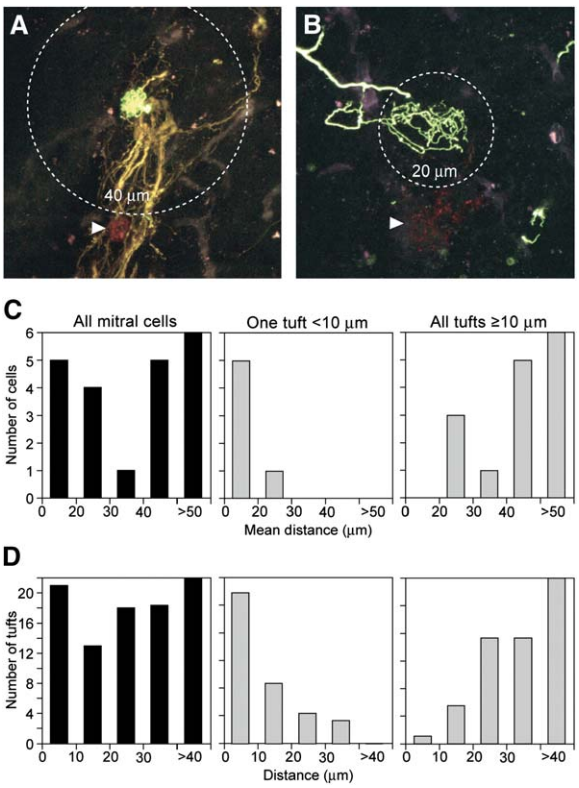

Figure 7. Analysis of Distances from Dye-Filled Dendritic Tufts to Genetically Labeled Glomeruli Defines Two Populations of Mitral Cells with Different Tuft Location Preferences

(A) An AF488-injected tuft contacts an YFP-labeled glomerulus and lays 40 μm from a DsRed1-labeled glomerulus. The circle is centered on the injected tuft and reaches the border of the DsRed1 glomerulus.

(B) An AF488-injected tuft in a different preparation located 20 μm from a DsRed1-labeled glomerulus.

(C) For each mitral cell, the mean distance between each of its dendritic tufts and the closest *V1Ra1/3* glomerulus. Results for all cells (left) reveal a bimodal distribution that can be differentiated by separating cells with at least one tuft within 10 μm of a *V1Ra1/3* glomerulus (middle) from those with no tufts within 10 μm (right).

(D) Distribution of distances from the closest *V1Ra1/3* glomerulus to individual dye-filled dendritic tufts of the cells plotted as in (C), showing a clear preference for tufts of cells from the first group (middle) to be located near *V1Ra1/3* glomeruli in contrast to tufts of cells from the second group (right).

defined by the location of their dendritic arbor relative to *V1Ra1* or *V1Ra3* glomeruli. The first population displays a mean distance from dendritic tufts to labeled glomeruli of less than 30 μm, while the second shows an average distance of greater than 40 μm. To better understand the difference between the two sets of mitral cells, we separately analyzed mitral cells with at least one tuft adjacent to (i.e., located less than 10 μm from) a labeled *V1Ra* glomerulus (Figure 7C, middle) and those with no adjacent tufts (all tufts at least 10 μm away) (Figure 7C, right). Five out of six (83%) cells in the first category have a mean distance of less than 20 μm, whereas 12 out of 15 (80%) of the latter cells have a mean distance greater than 40 μm. One cell in the first category and three cells in the second have an average distance between 20 μm and 40 μm. The statistical difference between these groups is highly significant ($p < 0.00001$, one-tailed unpaired t test). These data suggest that, although mitral cells project dendrites that extend over the entire glomerular layer, one can distinguish specific populations of mitral cells, the dendrites of which are preferentially located in close proximity to glomerular inputs of related receptors.

To get a better idea of the homogeneity of mitral cells' dendritic arbors, we plotted the distribution of distances from individual tufts to the nearest labeled *V1Ra* glomerulus across all labeled cells and within each of the two identified populations. As seen in Figure 7D, 28 out of 35 (80%) tufts from cells with an adjacent labeled glomerulus (middle) are located less than 20 μm from a *V1Ra1/3* glomerulus, whereas 51 out of 56 (91%) dendritic tufts from cells with no adjacent glomerulus (right) are located more than 20 μm away. The statistical difference between these populations is highly significant ($p < 0.00001$, one-tailed unpaired t test). In contrast, the data from all cells (left) is evenly distributed. Thus, we conclude that if one dendritic tuft of a given AOB mitral cell terminates in close proximity to a *V1Ra1/3* glomerulus, most of its other tufts will as well, whether or not they are located in the same domain. Taken together, our results are consistent with the selective heterotypic model applied to a subfamily-based grid in the AOB glomerular layer, according to which mitral cells project dendrites to specific locations where they receive input from VNO neurons expressing closely related *V1R* genes.

Discussion

Sensory maps are topographic organizations of sensory inputs in the brain that generate an internal representation of external stimuli. In order to gain insight into the coding of pheromone signals by the vomeronasal system, we have examined the organizational principles of the map of *V1R* receptor activation in the brain and the underlying logic according to which the vomeronasal map is processed, or read, by the output neurons of the AOB, the mitral cells. Results described here are consistent with a general wiring diagram in which the organization of VNO inputs to the anterior AOB and their detection by mitral cells is based on the molecular subdivision of vomeronasal receptors into distinct groups of closely related *V1R* sequences, or subfamilies, rather than on the individual identity of each *V1R* sequence. This logic of sensory representation differs from the individual OR-based labeled lines of information flow used in the main olfactory system and has significant implications for the understanding of information processing of pheromone signals in the vomeronasal system.

Molecular Features Are the Basis for Olfactory Sensory Maps

In the visual and somatosensory systems, the topographic representation of sensory inputs in the brain reflects the spatial distribution of sensory receptor cells. This does not, however, apply to the olfactory or vomeronasal systems in which, except for a rough segregation of receptor expression into large zones of the MOE and VNO sensory epithelia (Herrada and Dulac, 1997; Ressler et al., 1993; Vassar et al., 1993), sensory cells are randomly scattered in the sensory neuroepithelium. Instead, the topographic organization of sensory

projections in the MOB and AOB was shown to reflect the molecular identity of the sensory receptors. In both systems, sensory neurons expressing a given receptor, although randomly dispersed throughout the neuroepithelium, project to specific loci, or glomeruli, in the main and accessory olfactory bulbs (Belluscio et al., 1999; Del Punta et al., 2002; Mombaerts, 1996). This mode of projection generates a map of receptor activation that is used by the brain to encode the detection of chemical cues. The existence of topographic sensory maps based upon the molecular characteristics of the receptor cells raises the issue of the transformation of molecular features into spatial information. The detailed mechanisms guiding the innervation of MOB glomeruli by neurons expressing specific receptors are not fully understood, although the critical role of the receptor molecule itself in determining such connections has been clearly demonstrated (Belluscio et al., 2002; Wang et al., 1998). In addition, several studies have shown that the axonal projections of neurons expressing highly homologous receptors are likely to be located in the same vicinity (Conzelmann et al., 2001; Strotmann et al., 1999, 2000). Interestingly, the sequence similarity between MOE receptors can be seen as analogous to the positional similarity between retinal ganglion cells. Assuming that closely related odorant receptors are likely to recognize structurally similar ligands, one can therefore predict that related chemical cues should activate adjacent areas in the MOB. Indeed, recent experiments have supported the existence of "molecular-feature domains" in the MOB, which are determined by primary features such as the functional group of the odorant and arranged according to secondary features like carbon-chain length (Mori et al., 2006). Such a higher-order organizational principle has yet to be described in the vomeronasal system.

BAC Transgenesis and the AOB Receptor Map

In the MOE, specific populations of sensory neurons, each expressing a given receptor, innervate only one or a few glomeruli at fixed positions on each side of the MOB (Mombaerts, 1996; Ressler et al., 1994; Vassar et al., 1994). This organization of sensory projections generates two simple symmetrical maps of OR activation in the brain in which the representation of each input is invariant and highly localized.

In contrast, VNO sensory neurons expressing the same receptor innervate multiple small glomeruli distributed throughout the AOB glomerular layer (Belluscio et al., 1999; Del Punta et al., 2002; Rodriguez et al., 1999), and the representation of VNO inputs associated with a specific receptor appears to be only loosely conserved between individual animals. The apparent complexity, together with the lack of clear stereotypy of the VNO receptor map, is difficult to reconcile with the neural constraints likely associated with the control of fixed, species-specific and genetically preprogrammed behavioral responses. We therefore reasoned that a higher organizational principle may exist that had not been identified in previous studies and that may transform the seemingly disordered projection patterns into an ordered receptor map. In order to unravel such an organization, we used genetic and imaging tools to perform a large-scale analysis of VNO sensory connectivity to the brain. We took advantage of the fact that multiple *V1Ra* and *V1Rb* genes are clustered together in the mouse genome in order to modify the loci of several *V1R* receptors in a single BAC. This led us to generate a transgenic mouse line in which distinct reporter cassettes (YFP, DsRed1, and CFP) were inserted into the loci of three *V1R*s genes (*V1Ra1*, *V1Ra3*, and *V1Rb1*, respectively) and to successfully identify three independent neuronal populations in the apical zone of the VNO neuroepithelium and their projections to the brain. The cross of the transgenic line with mouse lines in which the same or different receptor loci had been modified by homologous recombination demonstrated that endogenous mechanisms for receptor choice, including allelic restriction, and projection to appropriate glomerular targets remain intact. Hypothetically, it remains possible that VNO neurons expressing the endogenous wild-type allele innervate different glomeruli than those innervated by neurons expressing modified alleles. Although this possibility cannot be directly challenged in the AOB, we consider it highly unlikely from transgenic and targeting approaches performed in the main olfactory system, where it has been possible to directly compare the positions of wild-type and genetically labeled glomeruli by in situ hybridization on MOB sections (Mombaerts et al., 1996).

Organizational Principles of the AOB

Glomerular Layer

By differentially labeling several members of the *V1R* gene family in the same transgenic mouse line, we were able to uncover new guiding principles for the vomeronasal sensory representation in the brain. In the MOB, inputs from highly similar ORs are mapped onto adjacent glomeruli in a topographical order reflecting molecular features of their ligands (Mori et al., 2006). This arrangement provides a spatial code for odor detection such that the coordinates of an activated glomerulus are predictive of the odorant stimulus and the stimulated OR. In contrast, the organization of the AOB is dramatically different. Our data show that glomeruli innervated by two members of the *V1Ra* subfamily are intermingled within a few large domains in fixed positions in the AOB glomerular layer, while neurons expressing a member of the *V1Rb* subfamily send inputs to different domains that maintain fixed relative distances to the *V1Ra*-related domains. Similarly, analysis of glomerular projections from genetically labeled *V1Rh7*-, *V1Rh15*-, and *V1Re4*-expressing neurons in transgenic mouse lines showed shared projection coordinates for neurons expressing members of the *V1Rh* subfamily that are distinct from those of *V1Re*, *V1Ra*, and *V1Rb*. Thus, instead of the spatially ordered distribution of glomerular positions in the MOB, which reflects the continuous *OR* sequence variation and correlated change in molecular features of OR ligands, AOB innervation appears to be organized in clusters or domains that mirror the sequence clustering of *V1R* genes into phylogenetically divergent clades. In an additional contrast with the *OR* glomerular map of the MOB, the *V1R* map of the AOB appears repetitive: each subfamily-related domain is present several times in separate locations in the AOB, and each subfamily-based domain contains numerous glomeruli corresponding to an individual receptor.

Moreover, multiple glomeruli representing identical and different receptors of the same subfamily are intermingled within each domain with no apparent intradomain spatial order. Hence, while the MOB sensory map is highly predictive and generates a fine spatial code where the location of a signal bears information regarding the precise nature of the stimulus, the AOB map provides instead an identity code (Laurent, 1999) such that the location of a signal is only broadly predictive of a group of cues associated with a particular receptor subfamily. An earlier study of projections of individual *V1R* receptors had postulated that each domain may correspond to an individual functional unit (Belluscio et al., 1999). Our data now suggest that domains of the AOB glomerular layer bring together information from highly related receptors.

The Sensory Logic of AOB Mitral Cell Connectivity

Using random intracellular dye injections into AOB mitral cells of SW3M mice, we showed that mitral cells establishing synapses with *V1Ra1*- and *V1Ra3*-expressing neurons also send dendrites to glomeruli associated with other receptors. In addition, we observed that mitral cells with dendritic tufts within or very close to a *V1Ra1* or *V1Ra3* glomerulus tend to project most, if not all, of their other dendrites toward the vicinity of *V1Ra1* and *V1Ra3* glomeruli, including those in distant domains across the anterior AOB. Thus, the dendritic arbors of mitral cells, although apparently randomly spread across large distances of the AOB glomerular layer, seem to in fact obey specific spatial and molecular constraints in establishing their connectivity. The dendritic innervation of glomeruli of different types clustered around *V1Ra1* and *V1Ra3* glomeruli supports the idea that AOB mitral cells tend to restrict their dendritic connectivity to specific glomerular domains associated with receptor subfamilies. This hypothesis appears directly confirmed by the identification in our study of a mitral cell integrating inputs from two members of the *V1Ra* subfamily. Thus, rather than simple homotypic or random heterotypic connectivity, AOB mitral cells instead exhibit a selective heterotypic dendritic connectivity that may at least partially follow the boundaries of receptor subfamilies. An earlier study (Del Punta et al., 2002) reported the presence of exclusively homotypic connections between mitral cells and genetically labeled glomeruli, suggesting to the authors that, despite its apparent dissimilarity, the underlying wiring scheme of AOB connectivity may be identical to that of the MOB. Several factors may account for the discrepancy between those earlier results and our data, including differences in experimental approaches and in the nature of the genetically modified receptor loci. We exclude the possibility that differences resulted from the modification of receptor loci by gene targeting (Del Punta et al., 2002) versus BAC transgenesis (our approach) because we have demonstrated that all genetically-labeled glomeruli show expression of dual reporter genes in crosses of SW1M or SW3M transgenic lines with the VN12/T40 line obtained by homologous recombination. A more relevant difference may reside in the labeling of mitral cell dendrites by intracellular dye injections into mitral cell bodies held in whole-cell patch-clamp configuration (our study) as compared to lipophilic dye injections into labeled glomeruli (Del Punta et al., 2002). Intracellular dye injection exclusively labels the injected cell, and we took great care to ensure that only one cell was injected with a particular dye in each preparation by inspecting the injected cell after each injection and before fixation. Out of 150 injected mitral cells, we never encountered the dye-coupling or labeling of more that one cell per injection. Hence, we conclude with confidence that all dendritic tufts labeled with a certain dye are part of the same mitral cell, even when split between several slices of the same preparation. In contrast, lipophilic dye labels cells by contact and may lead to unintended labeling and confounding results. Finally, it is also possible that different rules of connectivity are followed by different *V1R*s or *V1R* subfamilies. Genetic modification of additional *V1R* loci and the development of new methods for tracing AOB mitral cell dendrites may clarify this point in the future.

A Unifying Scheme of Pheromone Sensory Processing

Pheromone detection plays a role in a variety of intraspecies recognition processes ranging from sex identification leading to mating or aggression (Leypold et al., 2002; Stowers et al., 2002) to more subtle recognition of individual identity as shown in the Bruce effect (Gangrade and Dominic, 1984; Kaba et al., 1989; Kumar and Dominic, 1993). It is unclear whether vomeronasal responses rely on the presence of individual chemicals or blends of pheromonal cues. Single, behaviorally active pheromonal cues have been identified in mating and suckling behaviors in rodents (Lin da et al., 2005; Schaal et al., 2003) while the specific recognition of pheromonal blends with distinct concentration ratios of the same components has been well documented in fish and insects (Hildebrand, 1995; Sorensen et al., 1998). Homotypic connectivity of mitral cells to single glomeruli, as demonstrated in the MOB, is likely to facilitate the detection and discrimination of individual chemical compounds with integration of information from multiple receptors carried out largely at higher cortical relay stations (Zou and Buck, 2006). In contrast, the heterotypic connectivity demonstrated with AOB mitral cells seems particularly appropriate for detection of pheromonal blends. Unlike information originating from the MOB that can be further processed by multiple cortical areas, the AOB projects directly to behaviorally relevant areas of the amygdala where inputs from both the anterior and posterior AOB (i.e., originating from *V1R* and *V2R* receptor activation) were shown to converge on the same nuclei (von Campenhausen and Mori, 2000). Thus, local integration of *V1R*-related information may already largely occur within the anterior AOB. Extracellular recordings from AOB mitral cells in behaving mice (Luo et al., 2003) have shown extremely specific responses to natural stimuli with spikes induced by only one out of six mouse odors originating from various strains and genders. This specificity of response to complex stimuli may result from the presence of a single distinct cue in each of the stimuli or may be generated by the integration of blends of chemicals in various ratios, a scenario shown in the moth to enable species recognition by a balance between excitatory and inhibitory inputs rather than by a single type of excitatory input.

Our results indicate that the AOB glomerular map, as well as the dendritic connections of AOB mitral cells to this map, is organized according to the subdivision of *V1R*s into discrete and divergent subfamilies. This design is likely to facilitate integration of, and discrimination between, highly similar ligands, a process that may be highly relevant in pheromone recognition leading to specific behavioral responses. In insects and fish, pheromone detection leading to species, gender, and individual recognition has been shown to involve highly related chemical compounds such as steroids and steroid metabolites or multiple aldehydes of a specific length. Similarly, molecules with proven pheromonal activity in mammals are highly structurally related (Dulac and Torello, 2003). Pheromone recognition across animal species seems therefore to rely on chemical strategies that provide high redundancy with potential for subtle discrimination. High redundancy would ensure that energy-consuming behaviors such as aggression or mating are not triggered unless multiple related chemicals, for example testosterone and several of its metabolites which all signal a male, are coincidentally detected. Furthermore, as shown in insects, relative ratios of highly related chemicals provide an efficient chemical code to discriminate between closely related individuals. We propose that the distinctive features of the AOB glomerular map uncovered in our study have been selected to provide a sensory representation of pheromonal blends with specific ratios of structurally related chemicals.

Experimental Procedures

Generation of SW1M Mice

A C57BL/6j BAC array (RPCI-23, segment 2) was screened for *V1Ra/b*-containing BACs. BAC 398H20 was chosen for modification. *PstI* fragments of this BAC containing six of the seven *V1Ra/b* genes included in the BAC (excluding *V1Ra1*) were subcloned and sequenced. The *tau-lacZ-LNL* cassette was excised from the ETLpA-/LNL plasmid (Mombaerts et al., 1996) and replaced with *EYFP* coding sequence from pEYFP-C1 (Clontech) to create the ITYFP plasmid. The *ITYFP* cassette was inserted into the VN12 plasmid (Belluscio et al., 1999) to create VN12-ITYFP. The *VN12-ITYFP* cassette was transferred to pSV-RecA to create pSV-VN12-ITYFP, which was used to modify BAC 398H20 into BAC SW1M using methods previously described (Yang et al., 1997). Pronuclear injection of BAC SW1M yielded the SW1M transgenic mouse line.

Generation of SW3M Mice

ECFP was subcloned into the ETLpA-/LNL plasmid as described for *EYFP* to create the ITCFP plasmid. The *ITCFP* cassette was inserted into the VN2 plasmid (Belluscio et al., 1999) to create VN2-ITCFP. The *VN2-ITCFP* cassette was transferred to pSV-RecA to create pSV-VN2-ITCFP, which was used to generate BAC SW2M from BAC SW1M. A 2kb fragment including the *V1Ra3* gene was subcloned into a modified pBluescript-KS(-) plasmid (Stratagene) to create pBS-Pst4. The *IRES-vamp2-DsRed1* cassette from the IVR plasmid (gift of Dr. E. Chang) was inserted into pBS-Pst4 to create Pst4-IVR. The *Pst4-IVR* cassette was transferred to pSV-RecA to create pSV-Pst4-IVR, which was used to generate BAC SW3M from BAC SW2M.

Generation of V1Re4-ITG-, V1Rh7-ITY-, and V1Rh15-ITC-Labeled Mouse Lines

BACs containing each of the three receptor genes were identified: RP23-228E17 for *V1Re4*, RP23-301O3 for *V1Rh7*, and RP23-263D15 for *V1Rh15*. 5′ and 3′ homology arms for each receptor containing a total 1 kb of sequence centered on the stop codon were amplified from these BACs and cloned into a modified version of pBS-SK(+). The *ITYFP* and *ITCFP* cassettes described above, as well as a similar *ITGFP* cassette derived from *EGFP* coding sequence (Clontech), were inserted between the receptor homology arms as follows: *ITGFP* for *V1Re4*, *ITYFP* for *V1Rh7*, and *ITCFP* for *V1Rh15*. The *IRES-tau*-fluorescent protein cassettes flanked by receptor homology arms were transferred to pSV-RecA to generate the three constructs subsequently used for BAC modification and generation of transgenic mouse lines.

Immunocytochemistry

Anaesthetized mice were perfused with cold 0.1 M phosphate buffer (PBS) followed by 4% paraformaldehyde (PFA). Olfactory bulbs were embedded in 4% agarose and sliced parasagittaly at 50 μm or 100 μm using a VT1000S vibratome (Leica). Slices were treated according to standard histochemistry protocols. Primary antibodies against β-galactosidase (goat polyclonal, Cappel) and GFP (Molecular Probes) were used (1:500) at 4ºC overnight. CY3-conjugated anti-goat (1:200, Jackson Immunoresearch) and Alexa Fluor 488-conjugated anti-rabbit (1:500, Molecular Probes) secondary antibodies were used for 45 min at room temperature (RT) or 4 hr at 4ºC.

Glomerular Map Analysis

Olfactory bulbs were dissected and embedded as described above. 100 μm slices were made using a 752M Vibroslice (Campden Inst.).

Intracellular Injection of Mitral Cells

Adult SW3M mice were anaesthetized and decapitated. Olfactory bulbs were dissected out into a solution containing the following (in mM): 110 choline-Cl, 25 $NaHCO_3$, 25 glucose, 11.5 Na-ascorbate, 7 $MgSO_4$, 3.1 Na-pyruvate, 2.5 KCl, 1.25 NaH_2PO_4, and 0.5 $CaCl_2$. Bulbs were embedded in agarose and sliced parasagittally or as described (Del Punta et al., 2002) for semicoronal slices. Four hundred micrometer slices were equilibrated for at least 1 hr in a solution containing the following(in mM): 125 NaCl, 25 $NaHCO_3$, 15 glucose, 3 KCl, 2 $CaCl_2$, 1.3 NaH_2PO_4, and 1 $MgCl_2$. Patch-clamping of mitral cells was done under infrared video microscopy using glass electrodes filled with 0.5 mg/ml lucifer yellow (lithium salt, Sigma), Alexa Fluor 488, or Alexa Fluor 568 (sodium salt, Molecular Probes) dissolved in 150 mM KCl and 10 mM HEPES (pH 7.4). After achieving whole-cell patch-clamp configuration, 10–100 pA negative current steps (50 ms, 4 Hz) were applied for 10 min and 30 min for the Alexa Fluors and lucifer yellow, respectively. Slices were inspected using a CFP/YFP/DsRed filter set (61008, Chroma) after each injection and at the end of the experiment to ensure that only one cell was injected with each dye. Preparations were fixed in 4% PFA (30 min) and either embedded in 4% agarose and sliced at 100 μm (first set of experiments) or slowly compressed to ~100 μm (second set of experiments).

Supplemental Data

The Supplemental Data for this article can be found online at http://www.neuron.org/cgi/content/full/50/5/697/DC1/.

Acknowledgments

We thank R. Hellmiss for artistic work, J. Dubauskaite for mouse transgenics, Drs. J. Lichtman and J. Tapia for advice on imaging techniques, Dr. N. Book for excellent technical assistance, Drs. Y. Yarom and A. Mizrahi for their generous help, and the Dulac lab for helpful discussions and comments on the manuscript. This work was supported by the Howard Hughes Medical Institute (C.D.), the National Institute for Psychobiology in Israel (S.W.), the Interdisciplinary Center for Computational Neuroscience of the Hebrew University, Jerusalem (S.W.), NIH-NIDCD grant R01 DC003903 (C.D.), and EMBO long-term fellowship # 283-1998 (S.W.).

Received: February 24, 2006
Revised: April 17, 2006
Accepted: April 26, 2006
Published: May 31, 2006

References

Belluscio, L., Koentges, G., Axel, R., and Dulac, C. (1999). A map of pheromone receptor activation in the mammalian brain. Cell *97*, 209–220.

Belluscio, L., Lodovichi, C., Feinstein, P., Mombaerts, P., and Katz, L.C. (2002). Odorant receptors instruct functional circuitry in the mouse olfactory bulb. Nature *419*, 296–300.

Boehm, U., Zou, Z., and Buck, L.B. (2005). Feedback loops link odor and pheromone signaling with reproduction. Cell *123*, 683–695.

Chess, A., Simon, I., Cedar, H., and Axel, R. (1994). Allelic inactivation regulates olfactory receptor gene expression. Cell *78*, 823–834.

Conzelmann, S., Malun, D., Breer, H., and Strotmann, J. (2001). Brain targeting and glomerulus formation of two olfactory neuron populations expressing related receptor types. Eur. J. Neurosci. *14*, 1623–1632.

Del Punta, K., Puche, A., Adams, N.C., Rodriguez, I., and Mombaerts, P. (2002). A divergent pattern of sensory axonal projections is rendered convergent by second-order neurons in the accessory olfactory bulb. Neuron *35*, 1057–1066.

Dulac, C. (2005). Molecular architecture of pheromone sensing in mammals. Novartis Found. Symp. *268*, 100–107.

Dulac, C., and Torello, A.T. (2003). Molecular detection of pheromone signals in mammals: from genes to behaviour. Nat. Rev. Neurosci. *4*, 551–562.

Gangrade, B.K., and Dominic, C.J. (1984). Studies of the male-originating pheromones involved in the Whitten effect and Bruce effect in mice. Biol. Reprod. *31*, 89–96.

Herrada, G., and Dulac, C. (1997). A novel family of putative pheromone receptors in mammals with a topographically organized and sexually dimorphic distribution. Cell *90*, 763–773.

Hildebrand, J.G. (1995). Analysis of chemical signals by nervous systems. Proc. Natl. Acad. Sci. USA *92*, 67–74.

Kaba, H., Rosser, A., and Keverne, B. (1989). Neural basis of olfactory memory in the context of pregnancy block. Neuroscience *32*, 657–662.

Kanzaki, R., Arbas, E.A., Strausfeld, N.J., and Hildebrand, J.G. (1989). Physiology and morphology of projection neurons in the antennal lobe of the male moth Manduca sexta. J. Comp. Physiol. [A] *165*, 427–453.

Kumar, A., and Dominic, C.J. (1993). Male-induced implantation failure (the Bruce effect) in mice: protective effect of familiar males on implantation. Physiol. Behav. *54*, 1169–1172.

Laurent, G. (1999). A systems perspective on early olfactory coding. Science *286*, 723–728.

Leypold, B.G., Yu, C.R., Leinders-Zufall, T., Kim, M.M., Zufall, F., and Axel, R. (2002). Altered sexual and social behaviors in trp2 mutant mice. Proc. Natl. Acad. Sci. USA *99*, 6376–6381.

Lin da, Y., Zhang, S.Z., Block, E., and Katz, L.C. (2005). Encoding social signals in the mouse main olfactory bulb. Nature *434*, 470–477.

Luo, M., and Katz, L.C. (2004). Encoding pheromonal signals in the mammalian vomeronasal system. Curr. Opin. Neurobiol. *14*, 428–434.

Luo, M., Fee, M.S., and Katz, L.C. (2003). Encoding pheromonal signals in the accessory olfactory bulb of behaving mice. Science *299*, 1196–1201.

Mandiyan, V.S., Coats, J.K., and Shah, N.M. (2005). Deficits in sexual and aggressive behaviors in Cnga2 mutant mice. Nat. Neurosci. *8*, 1660–1662.

Mombaerts, P. (1996). Targeting olfaction. Curr. Opin. Neurobiol. *6*, 481–486.

Mombaerts, P., Wang, F., Dulac, C., Chao, S.K., Nemes, A., Mendelsohn, M., Edmondson, J., and Axel, R. (1996). Visualizing an olfactory sensory map. Cell *87*, 675–686.

Mori, K., Takahashi, Y.K., Igarashi, K.M., and Yamaguchi, M. (2006). Maps of odorant molecular features in the Mammalian olfactory bulb. Physiol. Rev. *86*, 409–433.

Ressler, K.J., Sullivan, S.L., and Buck, L.B. (1993). A zonal organization of odorant receptor gene expression in the olfactory epithelium. Cell *73*, 597–609.

Ressler, K.J., Sullivan, S.L., and Buck, L.B. (1994). Information coding in the olfactory system: evidence for a stereotyped and highly organized epitope map in the olfactory bulb. Cell *79*, 1245–1255.

Rodriguez, I., Feinstein, P., and Mombaerts, P. (1999). Variable patterns of axonal projections of sensory neurons in the mouse vomeronasal system. Cell *97*, 199–208.

Rodriguez, I., Del Punta, K., Rothman, A., Ishii, T., and Mombaerts, P. (2002). Multiple new and isolated families within the mouse superfamily of V1r vomeronasal receptors. Nat. Neurosci. *5*, 134–140.

Sadek, M.M., Hansson, B.S., Rospars, J.P., and Anton, S. (2002). Glomerular representation of plant volatiles and sex pheromone components in the antennal lobe of the female Spodoptera littoralis. J. Exp. Biol. *205*, 1363–1376.

Schaal, B., Coureaud, G., Langlois, D., Ginies, C., Semon, E., and Perrier, G. (2003). Chemical and behavioural characterization of the rabbit mammary pheromone. Nature *424*, 68–72.

Serizawa, S., Ishii, T., Nakatani, H., Tsuboi, A., Nagawa, F., Asano, M., Sudo, K., Sakagami, J., Sakano, H., Ijiri, T., et al. (2000). Mutually exclusive expression of odorant receptor transgenes. Nat. Neurosci. *3*, 687–693.

Sorensen, P.W., Christensen, T.A., and Stacey, N.E. (1998). Discrimination of pheromonal cues in fish: emerging parallels with insects. Curr. Opin. Neurobiol. *8*, 458–467.

Stowers, L., Holy, T.E., Meister, M., Dulac, C., and Koentges, G. (2002). Loss of sex discrimination and male-male aggression in mice deficient for TRP2. Science *295*, 1493–1500.

Strotmann, J., Hoppe, R., Conzelmann, S., Feinstein, P., Mombaerts, P., and Breer, H. (1999). Small subfamily of olfactory receptor genes: structural features, expression pattern and genomic organization. Gene *236*, 281–291.

Strotmann, J., Conzelmann, S., Beck, A., Feinstein, P., Breer, H., and Mombaerts, P. (2000). Local permutations in the glomerular array of the mouse olfactory bulb. J. Neurosci. *20*, 6927–6938.

Takami, S., and Graziadei, P.P. (1990). Morphological complexity of the glomerulus in the rat accessory olfactory bulb–a Golgi study. Brain Res. *510*, 339–342.

Tsuboi, A., Yoshihara, S., Yamazaki, N., Kasai, H., Asai-Tsuboi, H., Komatsu, M., Serizawa, S., Ishii, T., Matsuda, Y., Nagawa, F., and Sakano, H. (1999). Olfactory neurons expressing closely linked and homologous odorant receptor genes tend to project their axons to neighboring glomeruli on the olfactory bulb. J. Neurosci. *19*, 8409–8418.

Vassar, R., Ngai, J., and Axel, R. (1993). Spatial segregation of odorant receptor expression in the mammalian olfactory epithelium. Cell *74*, 309–318.

Vassar, R., Chao, S.K., Sitcheran, R., Nunez, J.M., Vosshall, L.B., and Axel, R. (1994). Topographic organization of sensory projections to the olfactory bulb. Cell *79*, 981–991.

Vickers, N.J., and Christensen, T.A. (2003). Functional divergence of spatially conserved olfactory glomeruli in two related moth species. Chem. Senses *28*, 325–338.

von Campenhausen, H., and Mori, K. (2000). Convergence of segregated pheromonal pathways from the accessory olfactory bulb to the cortex in the mouse. Eur. J. Neurosci. *12*, 33–46.

Wang, F., Nemes, A., Mendelsohn, M., and Axel, R. (1998). Odorant receptors govern the formation of a precise topographic map. Cell *93*, 47–60.

Yang, H., Shi, P., Zhang, Y.P., and Zhang, J. (2005). Composition and evolution of the V2r vomeronasal receptor gene repertoire in mice and rats. Genomics *86*, 306–315.

Yang, X.W., Model, P., and Heintz, N. (1997). Homologous recombination based modification in Escherichia coli and germline transmission in transgenic mice of a bacterial artificial chromosome. Nat. Biotechnol. *15*, 859–865.

Yoon, H., Enquist, L.W., and Dulac, C. (2005). Olfactory inputs to hypothalamic neurons controlling reproduction and fertility. Cell *123*, 669–682.

Zou, Z., and Buck, L.B. (2006). Combinatorial effects of odorant mixes in olfactory cortex. Science *311*, 1477–1481.